equation (3.4), clearly consists of polynomial terms only. That the influence of the geometrical parameter $\sigma = \frac{y}{x}$ on $P_t$, is dominant, as suggested by equation (3.6), is therefore true and is indeed confirmed by equation (3.8). (Note the mathematical predominance of the interrelated parameters d, x and y in equation (3.8). Also, the hypothesis advanced, which was based on the influence of $\sigma$, seem to be acceptable.

It now also became possible to derive an expression for $V_2$, at an appropriate value of $C_p$, from which $V_e$ and hence K' could probably be estimated for a given free-stream velocity $V_o$.

As shown in Appendix II, a quadratic equation for $V_2$ was derived, viz :

$$AV_2^2 + BV_2 + C = 0 \quad \ldots\ldots\ldots\ldots\ldots\ldots\ldots\ldots (3.9)$$

where ;

$$A = \left[\frac{\rho}{2} + \frac{2.4\rho}{nx^5}\right] ;$$

$$B = \left[\frac{32\mu\ell_1 y^2}{x^4} + \frac{32\mu\ \ell_2}{y^2}\right] \quad \text{and}$$

$$C = \tfrac{1}{2}\rho V_o^2 \left[C_p - 1\right]$$

From equation (3.9) ;

$$V_2 = \frac{-B \pm \sqrt{B^2 - 4AC}}{2A} \quad \text{............. (3.10)}$$

Thus, by substituting the dimensions of different probes to be tested in equation (3.10) and evaluating the parameters pertaining to the actual test conditions, $V_2$, $V_e$ and $K'$ can be calculated for different $\sigma$-values with a view to comparing experimental and theoretical probe performance.

The foregoing theoretical analysis does seem to indicate that $\sigma$ affects both the angular insensitivity range and the probe coefficient $K_\sigma$. Several fruitless attempts indicated that it did not seem possible to derive a relationship between $\sigma$ and angle of insensitivity because of the complex functional relationships and factors involved. On examining the fundamental expression for $P_t$, however, (equation 3.8) it became clear that $K_o$ could be expressed in terms of $\sigma$, and that it should therefore be possible to calculate $K_o$, uniquely, for a particular probe.

In Appendix II it is shown how equation (3.8) may be written as :

$$K_o = 1 - \frac{V_o^{\,2}}{P_t} \left\{ A_1 + (K')^2 \left[ \frac{G_1}{y^4} + \frac{G_2}{K'x^4} + \frac{G_3}{K'y^4} + \frac{G_4}{x^5} \right] \right\} \quad \text{.....(3.11)}$$

where :

$$A_1 = \frac{1}{2}\rho\left[C_p - 1\right] \quad ;$$

$$G_1 = \frac{1}{8}\rho d^4 \quad ;$$

$$G_2 = \frac{64\mu\, \ell_1 d^2}{V_o} \quad ;$$

$$G_3 = \frac{32\mu\, \ell_2 d^2}{V_o} \quad \text{and}$$

$$G_4 = \frac{4.8\,\rho\, \phi d^4}{\pi}$$

Thus, by applying equation (3.11), $K_o$ can be calculated in terms of $\sigma$, at any free-stream velocity $V_o$, for different parameter combinations of the same probe or for different probes, by using appropriate $C_p$-values.

In summarising, therefore, the theoretical analysis indicates :

(i) That the ratio $\sigma = \frac{y}{x}$ is the dominating theoretical probe parameter. This ratio is accordingly defined in terms of x and y, rather than d and y, to facilitate parameter changes while testing.

(ii) That the hypothesis advanced for establishing a mathematical model for flow through and round the spherical shield is reasonable and acceptable.

(iii) That the mathematical model reflects an effect of $\sigma$ on $K'$, and therefore on $V_e$ and conditions within the 'eddy reservoir' in the probe entrance which, in turn, should have a marked influence on angular insensitivity in positions of yaw and pitch, and

(iv) That $\sigma$ has a pronounced effect on the probe coefficient $K_o$.

3.3.1.3 Application of the theory developed to the probe in yaw and pitch

In the light of the theoretical conclusions formulated in paragraph (iii) above, the angular insensitivity characteristics of spherically shielded probes need further analysis.

Fig. 3.8(a) shows a diagrammatic sketch of the probe configuration assuming that its position of yaw in a free stream of velocity $V_o$ is such that the flow is inclined at an angle $\alpha$ to the shield axis in the direction of flow. The axial component of the velocity is therefore given by $V_o \cos\alpha$. If $\sigma$ assumes any value less than unity such that throttling takes place, $K'$ would be small and fractional whence $V_e$ can be written as :

$$V_e = K' V_o \cos\alpha \quad \text{.........................(3.12)}$$

(refer equation (3.7))

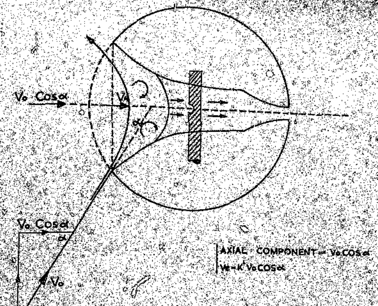


FIG. 3. 8. (a)

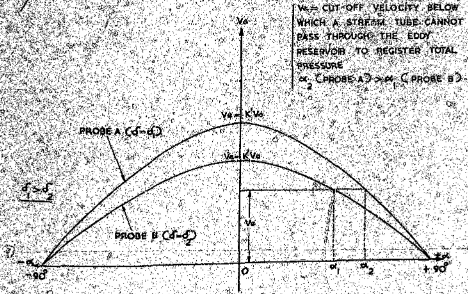


FIG. 3·8 (b) (DIAGRAMATIC)

It is clear from equation (3.12) that as $\alpha$ increases, $V_e$ decreases and would become very small for larger angles of yaw. Considering the 'eddy reservoir' or 'pressurised fluid cushion' theory, it seems logical to argue that an imaginary axial stream tube would be retarded by this 'cushion' but, in passing through it, would be accelerated again towards the venting orifice to render its total energy at the impact orifice in the central sting in the form of total pressure.

When the flow is oblique, however, and the probe is turned through larger angles of yaw, the axial component, $V_o \cos\alpha$, becomes so small that $V_e$, which is still smaller, could be totally masked by the 'eddy reservoir' or 'cushion' as shown by equation (3.12).

As outlined before, the principle embodied in shielded instruments is that of conservation of total energy along a streamline in loss-free flow. Total pressure can only be determined correctly, irrespective of flow direction, provided the stream tubes are deflected into the shield. When $V_e$ is therefore masked under the abovementioned conditions of yaw or pitch, the 'reservoir' or 'cushion' in the trumpet entry has become agitated by the oblique flow and does not allow the 'weakened' stream tube through to register its energy, but deflects it out of the probe as shown in the sketch. At this point one would expect the total pressure registered by the probe to fall sharply due to cutting off of the main flow through the probe. See Fig. 3.8(a).

This hypothesis could be compared with the functioning of an ordinary diode valve in electronics. If one imagines the 'eddy cushion' or 'reservoir' to act as a 'grid', it would pass through stream tubes in the same manner as a grid passes electrons in a valve, until the point is reached where the angle-of-flow inclination masks $V_e$ and hence imposes a 'cut-off' condition on the turbulent 'reservoir'. This prevents stream tubes from penetrating, in the same manner as the electron flow in a valve is terminated by the cut-off voltage on the grid.

In accordance with the theory expounded above, it can also be shown that the angle of insensitivity to flow direction is increased as $\sigma$ increases. Referring to Fig. 3.8(b), the relationship $V_e = K'V_o \cos\alpha$, for two identical probes differing only in diameter of venting orifice, may be illustrated graphically as shown. Probes A and B have $\sigma$-values of $\sigma_1$ and $\sigma_2$, respectively, where $\sigma_1 > \sigma_2$. The higher $\sigma$ value would, according to the theory, cause less throttling and hence a higher $K'$-value for the same free-stream velocity $V_o$. Thus, $V_e$ (probe A) $= K'V_o > V_e$ (probe B) $= K_1' V_o$. $(K' > K_1')$

as shown diagrammatically.

Furthermore, it can reasonably be assumed that, for two probes with identical dimensions differing only in size of the venting orifice diameter, the 'eddy reservoir' or 'cushion' formed in identical entrance diameters, d, at the same free-stream velocity, would impose a $V_s$-value at 'cut-off' which would be identical, or approximately so, for the two probes when subjected to oblique flow. If this $V_s$-value is denoted by $v_c$ in Fig. 3.8(b), it is clear that probe A would have a wider range of angular insensitivity to flow direction than probe B ($\alpha_2 > \alpha_1$).

3.3.2 Experimental procedure.

The foregoing theoretical analysis suggested the following experimental procedure.

3.3.2.1 Select a suitable shield diameter.

3.3.2.2 Select an initial size for probe entrance diameter, d. As stated earlier, the pressure distribution on the upstream face of a sphere for flow round it serves as a guide :

The pressure coefficient $C_p$ for a sphere can be defined as :

$$C_p = 1 - 9/4 \sin^2 \theta \quad \text{.......................(3.13)}$$

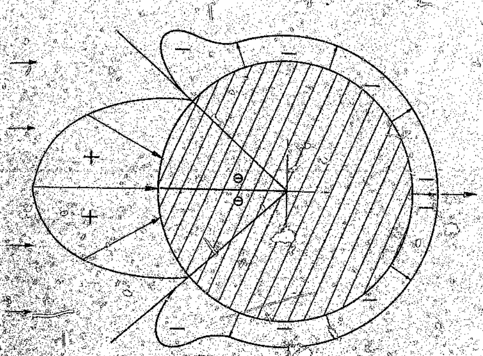

FIG. 3.9 PRESSURE DISTRIBUTION FOR FLOW ROUND A SPHERE

where $\theta$ is measured clockwise from the horizontal probe axis. See Fig. 3.9. If it is assumed that the entrance opening should not be bigger than the iris on which positive pressure exists, a probable value for d, in terms of D, is suggested which can be varied on test to determine the best value for $\frac{d}{D}$. The positive pressure iris is defined by the spherical circle on which $C_p = 0$. Therefore, from equation (3.13):

$$\sin^2 \theta = \frac{4}{9}$$

$$\therefore \quad \sin \theta = \frac{2}{3}$$

$$\text{also,} \quad \sin \theta = \frac{d}{D}$$

$$\therefore \quad \frac{d}{D} = \frac{2}{3} \quad \text{or} \quad d = \frac{2}{3}D$$

Hence if D is taken as 0.3 inch, d could be made approximately 0.2 inch for further experimental investigation.

3.3.2.3 Select values for x and $\phi$ such that reasonable transition between d and x is possible, and ensuring that the blockage effect of $\phi$ is negligible. Drill out different internal dimensions, subjecting combinations of d, x and $\phi$ to experimental testing, for constant y, and determine the best values for $\frac{d}{D}$ and $\frac{\phi}{x}$. The procedure to be adopted here should be dictated by experimental observation.

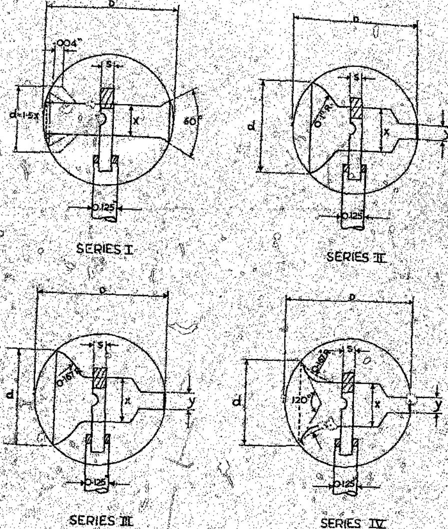


FIG. 3·10. TOTAL PRESSURE PROBES WITH SPHERICAL SHIELDS.

3.3.2.4 Vary the controlling parameters $\sigma$ and $R_e$ now and determine their influence.

3.3.2.5 The effect of $R_e$ could probably be eliminated by means of a trip wire or trip groove on the circumference of the sphere.

## 3.4 Tests on different designs of spherical shielded probes

In all, thirty-two versions of different design were tested in five test series; the details are given in Reference 4.

The basic designs tested are shown in Fig. 3.10 which illustrates the simplicity of construction.

In each instance, as shown in Fig. 3.10(a) and (b), the stem was press-fitted into the sphere; this made quick change-overs possible during tests. The spherical head was made from an araldite ball of diameter 0.3 inch. Following the guide given by the theoretical analysis, investigations were concentrated on the effects of entry shape, internal probe dimensions, and particularly the size of venting orifice.

### 3.4.1 Test facilities and method of testing

The following is a comprehensive summary. For details the reader is referred to Reference 4.

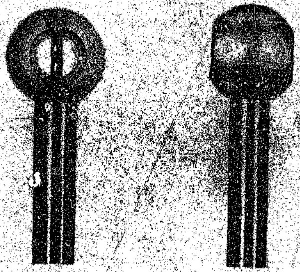

FIG. 3·10 (a) DETAILS OF PROBE CONSTRUCTION

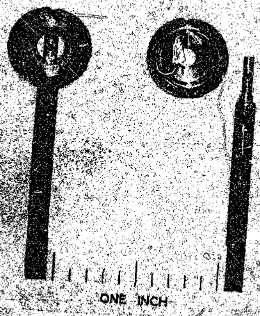


FIG. 3·10 (b) DETAILS OF PROBE CONSTRUCTION

The trial tests of test series I were conducted in a small blower tunnel with a 3-inch diameter jet; measurements of series II and III were carried out in an enclosed test section of 7.5 inch diameter, while for the final tests of series IV and V the 7.5 inch and 36 inch free jets of a large aerodynamic blower rig were employed. The distribution of velocities in the free jets and closed test section had previously been carefully examined and found to be suitably uniform. Uniformity of velocities is demonstrated by Fig. 3.11 in which is shown a tuft grid photographed at an air speed of 220 ft/sec.

The instruments on test were mounted in a standard carriage held in a special gimbal ring as shown in Fig. 3.12. Angles of yaw could be advanced in steps of one degree set by a protractor on the instrument carriage, while pitch settings, in 5-degree steps, could be chosen by locking the gimbal ring with a location pin which engaged accurately cut teeth on the periphery of a 'gear protractor'.

Readings were taken at constant air speeds in the range 70 ft/sec to 275 ft/sec and were referred to the centre-line record obtained for zero angle of attack. Results are presented as percentages of the centre-line dynamic pressure $q_c$. A total pressure reference probe

The trial tests of test series I were conducted in a small blower tunnel with a 3-inch diameter jet; measurements of series II and III were carried out in an enclosed test section of 7.5 inch diameter, while for the final tests of series IV and V the 7.5 inch and 36 inch free jets of a large aerodynamic blower rig were employed. The distribution of velocities in the free jets and closed test section had previously [illegible] fully examined and found to be suitably uniform. Uniformity of velocities is demonstrated by Fig. 3.11 in which [illegible] shown a tuft grid photographed at an air speed of 220 ft/sec.

The instruments on test were mounted in a standard carriage held in a special gimbal ring as shown in Fig. 3.12. Angles of yaw could be advanced in steps of one degree set by a protractor on the instrument carriage, while pitch settings, in 5-degree steps, could be chosen by locking the gimbal ring with a location pin which engaged accurately cut teeth on the periphery of a 'gear protractor'.

Readings were taken at constant air speeds in the range 70 ft/sec to 275 ft/sec and were referred to the centre-line record obtained for zero angle of attack. Results are presented as percentages of the centre-line dynamic pressure $q_c$. A total pr[illegible] reference probe

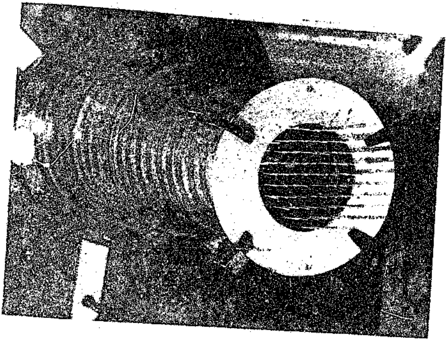

FIG. 3·11. 7·5 INCH FREE JET

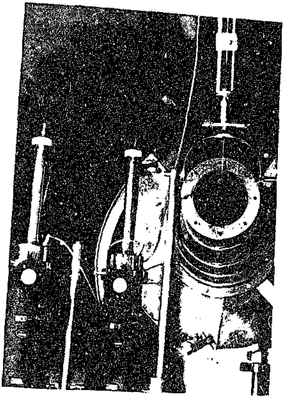

FIG. 3-12 PROBE MOUNTING

was mounted on the same elevation as the orifice of the probe on test (Fig. 3.12); once the latter was withdrawn from the test position on the horizontal axis of the gimbal ring, the reference probe reading could be taken at the same point; this arrangement was used to determine the probe coefficient. Yaw and pitch characteristics were established by using the instrument on test to record the reference pressure; repeated check readings were taken on the centre-line position during a test.

In test series I to III, during the initial development stages, probes were tested for yaw sensitivity only; in series IV, however, pitch readings were included, as also examination of the degree of constancy of the probe coefficient in the range 70 ft/sec to 275 ft/sec.

In addition, the response times were determined for the two final versions of the probe under suddenly applied air pressures of 500 mm water gauge.

3.4.2 Test results

In this sub-section the results, which are described in detail in reference 4, are summarised.

The experimental investigation aimed at developing a probe having a coefficient of unity, or as near unity as would be commensurate with the desired range of angular insensitivity, namely matching that of the miniature Kiel and cylindrical shielded probes.

In the trial test series an attempt was made to determine a reasonable dimension for x, in relation to a practical size of central sting hypodermic tube of diameter $\phi$.

In the second series, dimension x was kept constant while entrance diameter, d, and venting orifice size, y, were altered. An important aspect of this series was the experimental verification that the parameter, $\sigma = \frac{y}{x}$, has a controlling influence, as was predicted theoretically. See Fig. 3.10. Both range of insensitivity to angle-of-flow effects and instrument coefficient, $K_o$, are controlled by $\sigma$. Thus, for $\sigma \leq 0.41$, the coefficient is unity and for $\sigma$ = 0.4 to 0.41, yaw insensitivity extends to $\pm$ 30 degrees for a margin of accuracy of 1 per cent. If $\sigma$ = 1.0, the total pressure reading is correct to within 1 per cent over an angle of yaw of approximately $\pm$ 40 degrees but the probe coefficient is reduced to $K_o$ = 0.946, and varies with Reynolds number. This pattern of behaviour was confirmed in all subsequent experiments.

For test series III and IV the probe diameter was increased to 0.5 inch, and the probe shields were fabricated from phosphor-bronze ball-bearings, enabling the internal probe dimensions to be controlled more accurately than was possible with the 0.3 inch diameter araldite balls. Here d, $\sigma$, $\phi_i$ and size and finish of the impact orifice were varied with the object of optimising. The con[illegible] of $\sigma$ could be summarised as follows :

[illegible] $\sigma$ = 0.[illegible] to [illegible], $K_o$ = 1, and permissible [illegible] range is $\pm$ 30 degrees.

[illegible] $\sigma$ [illegible] $K_o$ = 1, but angular range decreases [illegible] below $\pm$ 30 degrees. For $\sigma >$ 0.[illegible], $K_o < 1$, and [illegible] with the Reynolds number, while permissible [illegible] increases with $\sigma$ to values above $\pm$ 30 [illegible] to a maximum of approximately 55 degrees at which [illegible] seems to be rather [illegible].

It was evident that [illegible] of an increased permissible angular range to be [illegible] increasing $\sigma$-values above 0.4, was offset by the disadvantage that $K_o$-values fall below unity and vary with Reynolds number.

Further improvement in manufacturing methods, use of more precise experimental matching of [illegible] dimensions and examination of the effect of a [illegible] groove in [illegible], led to the development of two [illegible] that [illegible] reasonable performance, viz : No. 2[illegible] and No. 2[illegible]. Figs. 3.13 and 3.14 show the characteristics of these

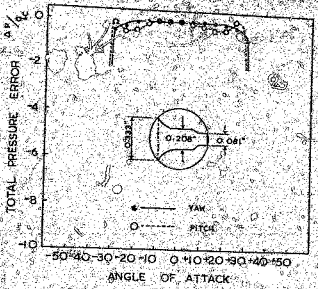


FIG. 3.13 VARIATION OF TOTAL PRESSURE ERROR WITH ANGLE OF ATTACK (INSTRUMENT NO. 26)

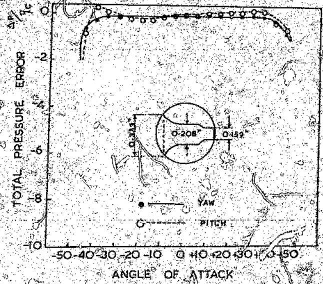


FIG. 3.14 VARIATION OF TOTAL PRESSURE ERROR WITH ANGLE OF ATTACK (INSTRUMENT NO. 28)

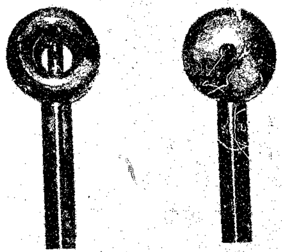

FIG. 3·15 (a) PROBE No. I

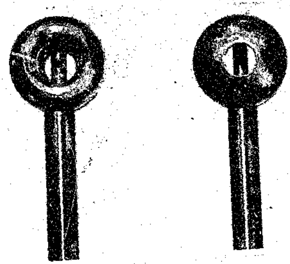

FIG. 3·15 (b) PROBE No. II.

FIG. 3·15 FINAL VERSION OF TOTAL-PRESSURE PROBE WITH SPHERICAL SHIELD

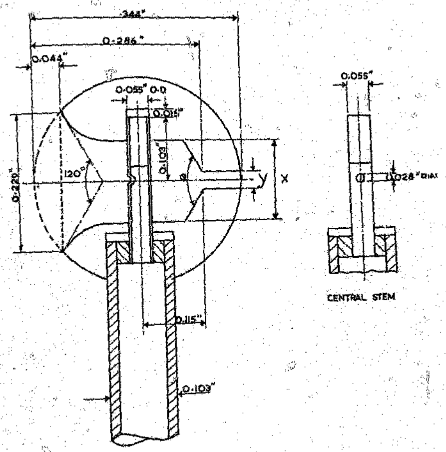


INSTRUMENT NO. I

$x = 0.144$
$y = 0.059$

INSTRUMENT NO. II

$x = 0.144$
$y = 0.110$

⊗ 120°-TIP OF STANDARD DRILL NO. 27

ENTRY OF SHIELD SHARPLY FLARED FROM 120°-CONE

ORIFICE FREE OF BURRS

FIG. 3.16 DIMENSIONS OF INSTRUMENTS NO. I AND NO. II probes.

To conclude the experimental work, scaled-down versions of these two instruments were made and tested in test series V.

### 3.5 Testing of versions conforming most closely to the desired characteristics

Fig. 3.15(a) and (b) and Fig. 3.16 show details of the finally adopted miniature probes which were tested on the large aerodynamic blower rig. Instrument characteristics are given in Figs. 3.17, 3.18, 3.19 and 3.20.

Of these, instrument No. I has a recovery coefficient of unity and a range of inclined flow insensitivity over ± 31 degrees of yaw and ± 30 degrees of pitch. The second probe, instrument No. II, has a coefficient of 0.991, which remains constant to within ± 0.2 per cent of dynamic pressure in the speed range 70 ft/sec to 275 ft/sec, (Fig. 3.21) while the insensitivity to flow direction extends to ± 48 degrees of yaw and ± 45 degrees of pitch for a margin of error of 1 per cent.

The best performance was obtained with probes having shielded entries sharply flared into a 120-degree 'trumpet' shape. [41] By using phosphor-bronze standard ball-bearing balls and cutting the internal contours with a special tool, the accurate manufacturing of these

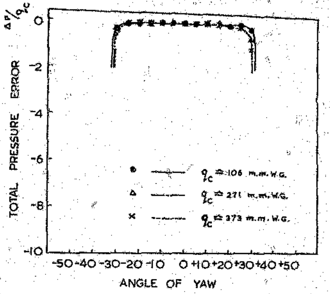


FIG. 3.17 VARIATION OF TOTAL PRESSURE ERROR WITH ANGLE OF YAW (INSTRUMENT NO. I)

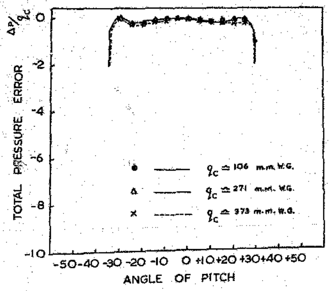


FIG. 3.18 VARIATION OF TOTAL PRESSURE ERROR WITH ANGLE OF PITCH (INSTRUMENT NO. I)

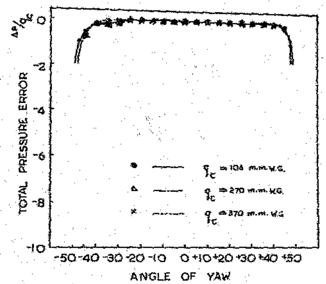


FIG.3.19 VARIATION OF TOTAL PRESSURE ERROR WITH ANGLE OF YAW (INSTRUMENT NO. II)

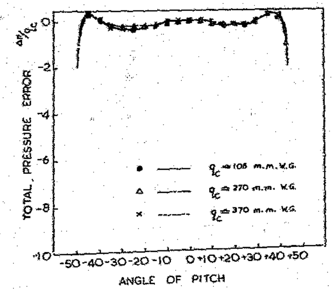


FIG.3.20 VARIATION OF TOTAL PRESSURE ERROR WITH ANGLE OF PITCH (INSTRUMENT NO. II)

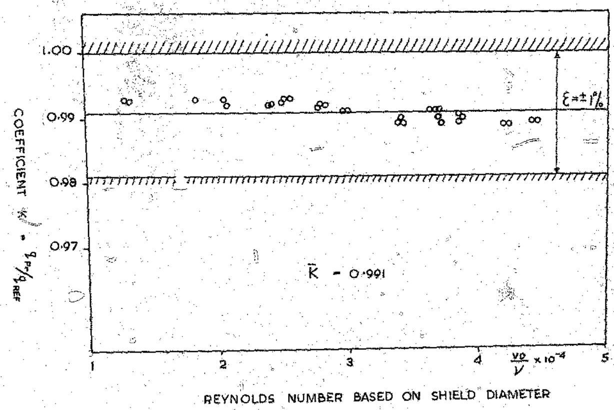


FIG. 3.21 DEPENDENCE OF PROBE COEFFICIENT ON REYNOLDS NUMBER (INSTRUMENT NO.11)

was considerably simplified.

These probes are structurally stiff and robust, and due to simplicity of design the response times were uniformly good, being 50 to 54 seconds under a suddenly applied air pressure of 500 mm water gauge.

The performance and characteristics of these miniature probes are therefore comparable to that of the original Kiel probe.

### 3.6 Comparison between theoretically derived flow characteristics and those observed during actual probe performance

#### 3.6.1 The effect of $\sigma$

Experiment confirmed the theoretical result that $\sigma = \frac{Y}{x}$ is the dominating geometrical probe parameter, and showed that probe performance is dependent on a critical $\sigma$-value of 0.4. This apparently critical experimental value will be re-examined later.

#### 3.6.2 The relationship between $\sigma$ and K' and the effect on angular insensitivity in yaw and pitch

By substituting the dimensions of different probes actually tested in equation (3.10) and evaluating the parameters pertaining to the test conditions, $V_2$, $V_e$ and K' can be calculated for different $\sigma$-values.

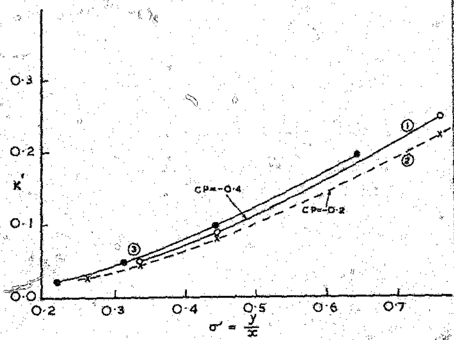


FIG. 3.22 THEORETICAL RELATION BETWEEN σ AND K'

The accepted value of $C_p$, the base pressure coefficient in the wake of a sphere, is -0.4. Because part of the flow is diverted through the spherical shield, however, it seems reasonable to assume that flow round the shield would differ from that round a whole sphere. Two values of $C_p$ were therefore used in the calculations, i.e. $C_p = -0.4$ and $C_p = -0.2$. At this stage it was thought that, use of different $C_p$-values might show up the effect of Reynolds number on probe performance.

The probe dimensions used, together with sample calculations, are shown in detail in Appendix III, Table III.1 and III.2. The results are given in graphical form in Fig. 3.22.

Graphs No. (1) and No. (2) represent K'-values as calculated for corresponding $\sigma$-values, for $C_p = -0.4$ and $C_p = -0.2$. These graphs lie fairly close together and show that Reynolds number effects become more marked the higher the $\sigma$-values; vide performance of probe No. II ($\sigma = 0.764$) compared with that of probe No. I ($\sigma = 0.41$). The graphs also show that $C_p$ is not highly critical.

To check these graphs, the general equation for $P_t$ (equation (3.8)) was evaluated directly. One of the tested probes having a sphere diameter of 0.34 inch with an x-value of 0.144 inch, was chosen at random. A $C_p$-value of -0.4 was adopted, while the value of $K_o$ for these probe dimensions was taken as determined experimentally, i.e. $K_o$ = 0.991. Values for the venting orifice diameter, y, were calculated for different assumed K'-values and these K'-values were plotted against the resulting theoretical σ-values. The results are shown in graph No. (3).

This method was adopted to accord with the experimental procedure of test series II, where the x-dimension was kept constant while the orifice diameter, y, was varied. It should be appreciated here that these theoretical σ-values were determined uniquely and that graph No. (3) therefore verifies graphs No. (1) and No. (2). Sample calculations are shown in Appendix III, Table III.3.

These graphs verify the hypothesis advanced originally, namely that as σ decreases - when flow through the probe is throttled - K' tends to z[illegible] and hence $V_e$ tends to zero - as shown by the equat[illegible] $V_e = K'V_o$ - associated with a corresponding static pressure rise. For the range of σ-values considered, K' and hence $V_e$ never reaches zero value, although it is clearly demonstrated that the flow is greatly retarded from a point in the free-stream, where the velocity is $V_o$, to the entrance zone of the probe where the velocity is $V_e$. Consequently, as originally hypothesized, the mathematical model simulates conditions prevailing when an 'eddy air cushion' forms a 'reservoir' under pressure in the trumpet entry zone of the probe.

On applying the above theory to probes in yaw or pitch it was shown, theoretically, that instruments with higher σ-values should have a wider range of insensitivity to flow direction than those with lower σ-values. (Probe A and probe B in Fig. 3.8(b)) Experimentally determined characteristics of probes No. I and No. II confirm this. Probe No. I has a σ-value of 0.41 and a insensitivity range of ± 30 degrees of yaw and pitch, while Probe No. II with a σ-value of 0.764, is insensitive to direction of flow over the range ± 48 degrees of yaw and ± 45 degrees of pitch. This is further proof of the validity of the hypothesis advanced.

### 3.6.3 Relationship between σ and $K_o$

Values for $K_o$ were calculated for different σ-values using $C_p$-values of -0.2 and -0.4 and actual probe dimensions in equation (3.11). The results are presented graphically by graphs No. (4) and No. (5) in Fig. 3.23. Sample calculations are given in Appendix III, Tabel III.4, and

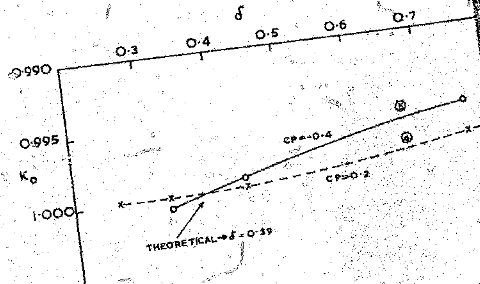


FIG 3·23 GRAPH δ vs $K_0$ (THEORETICAL)

Table III.5.

This result is remarkable : The graphs cross at a $\sigma$-value of $\approx 0.39$ and a $K_o$-value of approximately unity, graph No. (4) maintaining a $K_o$-value of near-unity for $\sigma$-values below 0.39. It also shows that a probe having a $\sigma$-value of approximately 0.39 would not be sensitive to changes in Reynolds number because $C_p$-values ranging from -0.2 to -0.4 do not affect the result. Further, it is clear that the point of crossing defines a critical $\sigma$-value of approximately 0.39. As $\sigma$ increases above this critical value, $K_o$ decreases to values below unity and, due to the departure of the curves, becomes increasingly dependent on Reynolds number. These results are an almost perfect verification of the experimental behaviour of probes No. I and No. II. Probe No. I ($\sigma = 0.41$) has a coefficient of unity for $\sigma$-values at and below 0.41, $K_o$ being independent of Reynolds number, while probe No. II ($\sigma = 0.764$) has a coefficient less than unity ($K_o = 0.991$), $K_o$ being increasingly dependent on Reynolds number, and decreasing below unity, as $\sigma$ is increased. The theoretically determined critical $\sigma$-value of 0.39 is almost identical to the experimental value of 0.40 to 0.41.

For a final comparison $K_o$ was predicted from equation (3.11) for instruments selected randomly from those tested. The experimentally determined average $K_o$-value for probe No. II was 0.991 at a σ-value of 0.764, while the average theoretical value for $C_p$ = -0.2 and -0.4 - was 0.997 - a discrepancy of 0.6 per cent. For other instruments the discrepancies between experimental and theoretical $K_o$-values lay between +1.2 and -0.01 per cent.

In the light of this manifestly satisfactory agreement between theory and experiment, it is submitted that the theoretical analysis is sound and the hypothesis advanced is acceptable. It has been shown that the mathematical model not only explains probe performance but also enables probe characteristics to be estimated.

### 3.7 Manufacturing of Probes

Experimental versions of the probe were made in two stages : For the spherical shield, Hoffmann standard-size bronze ball-bearing balls were used. These were held in a drilling vice by means of spherically counter-sunk slip blocks bearing marks by which the sphere centre could be located. Entry and venting orifices were drilled out and the inlet worked to the specified contour. The vice was then turned through 90 degrees and the stem holes drilled.

The stem was built up of stainless steel tubes, the

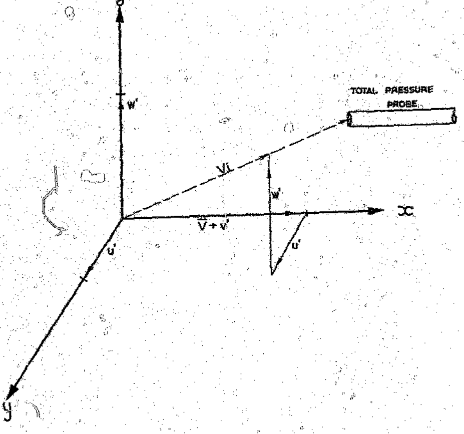


FIG. 3-23(a)TURBULENT FLOW DIAGRAM

tip portion of the inner cylinder being blocked, as indicated in Fig. 3.10, to reduce the small-bore volume to a minimum. The stem was then inserted into the shield and the total pressure orifice drilled exactly on centre-line with the aid of the slip block markings and an optical scanning device. Time taken to make one of the 0.34-inch diameter final version probes was just under five hours. Once dimensions are standardised a special cutting tool would enable the production time to be reduced to about 1½ hours.

## 4. FACTORS AFFECTING ACCURATE TOTAL PRESSURE MEASUREMENT

To improve the accuracy of total pressure measurement, the following factors must be analysed :

### 4.1 The effect of turbulence

In some fluid-flow problems the temporal mean velocity $\bar{V}$ is sought while in others, particularly those associated with turbo-machines and heat transfer, the true total pressure is required. An expression for true total pressure can be derived thus :

Referring to Fig. 3.23(a), the mean velocity $\bar{V}$ is assumed one-dimensional in the x-direction. The turbulent velocity fluctuations will be three-dimensional giving velocity components as shown. The bar denotes the time averaged mean values while the dashes in $v'$, $u'$ and $w'$ denote the instantaneous fluctuations from these mean values due to turbulence. The time averaged mean values of these fluctuating velocities are zero by definition.

True total pressure can be expressed as :

$$p_t = p_s + \tfrac{1}{2}\rho \, \overline{V_i^2} \qquad \ldots\ldots\ldots\ldots\ldots\ldots\ldots (3.14)$$

Figure 3.23(a) shows that :

$$V_i^2 = (\overline{V} + v')^2 + u'^2 + w'^2$$

$$= \overline{V}^2 + v'^2 + u'^2 + w'^2 \quad (2\overline{V}v' = o) \text{ and}$$

hence, according to definition :

$$\overline{V_i^2} = \overline{V}^2 + \overline{v'^2} + \overline{u'^2} + \overline{w'^2} \quad \ldots\ldots\ldots\ldots\ldots\ldots (3.15)$$

Substitution of equation (3.15) in equation (3.14) yields :

$$p_t = p_s + \tfrac{1}{2}\rho \, \overline{V}^2 + \tfrac{1}{2}\rho \, (\overline{v'^2} + \overline{u'^2} + \overline{w'^2}) \quad \ldots.(3.16)$$

In literature on the subject[(47)] one often finds the statement that the true total pressure, as defined by equation (3.16), is the pressure which an ordinary pitot tube actually measures. This statement is clearly incorrect. The ranges of angular insensitivity of the conventional pitot tubes and, to a certain degree, of the modified versions are totally inadequate to record the full instantaneous components of turbulent velocity fluctuations. It would be more nearly correct to state that these probes register :

$$p_t = p_s + \tfrac{1}{2}\rho\bar{V}^2 + \tfrac{1}{2}\Omega\rho\left[\overline{u'^2} + \overline{u'^2} + \overline{w'^2}\right] \text{.......}(3.17)$$

where $\Omega$ depends on the instrument's range of angular insensitivity and the degree of turbulence. Conventional total pressure probes do not register true total pressure as defined by equation (3.16) and at the same time the temporal mean velocity $\bar{V}$ determined by means of a total pressure probe in association with wall static tappings would be in error because $\Omega = 0$ in equation (3.16).

The characteristics of the spherical probe (instrument No. II), however, are such that this instrument would measure true total pressure in turbulent flows more accurately than conventional instruments because of its wide range of angular insensitivity. When used to determine the temporal mean velocity at a point, a correction factor should be applied to take care of the turbulent component of the total pressure registered. This correction factor can be determined as follows:

If $\Omega_t$ is the error coefficient due to turbulent components, then,

$$p_t = p_s + \tfrac{1}{2}\rho\bar{V}^2 + \tfrac{1}{2}\,\Omega_t\rho\,\overline{V^2} \text{ ................ } (3.18)$$

The true total pressure is given by equation (3.16) which can be written as :

$$P_t = p_s + \tfrac{1}{2}\rho\overline{V^2}\left[1 + \frac{\overline{v'^2} + \overline{u'^2} + \overline{w'^2}}{\overline{V^2}}\right] \quad \ldots\ldots(3.19)$$

Comparing equations (3.18) and (3.19) it is clear that :

$$\Omega_t = \left[\frac{\overline{v'^2} + \overline{u'^2} + \overline{w'^2}}{\overline{V^2}}\right]$$

Using the root mean square values of turbulent velocity fluctuations for a pipe, say, as determined by Laufer,[42] the magnitude of $\Omega_t$ for pipe flow can be evaluated. It should be pointed out, however, that appropriate total pressure corrections for turbulence in other flow situations are, at present, not possible owing to the lack of experimental data on the structure of turbulence. Determinations of r.m.s. values of turbulent velocity fluctuations, particularly near solid boundaries with the aid of the newly-developed 'hot-film' techniques, along with more detailed hot-wire anemometer surveys of a variety of flow fields are urgently required.

## 4.2 <u>The effect of swirl</u>

Swirl continues to present problems in flow measurement. Preston and Norbury [7] found that, in the case of a three-quarter radius meter with wall static tappings, a swirl constituting a 10 degree change in flow direction caused an error of 1 per cent in the discharge determination. They state that : 'The errors arising in a meter using pitot static tubes would depend on the yaw characteristics of the pitot static'. It would, of course, also depend on the range of angular insensitivity in 'pitch'.

Again it should be noted that the characteristics of the spherical probes are such that the effect of swirl would be minimised because of the relatively wide ranges of angular insensitivity.

## 4.3 Correction for probe centre line displacement

When a pressure probe is placed in a shear flow regime the pressure recorded is not that which actually acts at the point on the probe centre line.

Young and Maas (43) determined in a wake flow that for a blunt-nosed pitot tube having a ratio of hole to outside diameter of approximately 0.6, the effective centre of the probe was displaced a distance 0.18 times the outside diameter. Macmillan (44) reported that in boundary-layer flows such instruments also showed a wall proximity effect. On the other hand, Livesey (45) and Davies (46) have shown that displacement errors on sharp-lipped conical pitot tubes are very small.

This centre line displacement effect is a complicated problem which demands further attention. Displacement values for the spherically shielded probe have, as yet, not been investigated.

Oosthuizen [41] used the displacement factor of 0.18 as determined by Young and Maas [43] - which is not truly applicable because it was determined under 'outer region' conditions - to develop a relationship which defines the displacement as follows :

$$\frac{\overline{U_d}}{\overline{U}} = \sqrt{1 - \frac{dp}{D} \cdot \frac{0.72g'}{\sqrt{\frac{2}{C_f}} + 4 - g}} \quad \text{........(3.20)}$$

where $\overline{U_d}$ = true measured velocity due to displacement;

$\overline{U}$ = true velocity at point on centre line of probe;

$d_p$ = diameter of probe;

$D$ = duct diameter;

$C_f$ = local coefficient of skin friction;

$g$ = function describing turbulent velocity distribution in the 'outer region' in pipe flow;

$g'$ = the derivative of the above function.

$C_f$ is functionally related to $R_D$, the pipe Reynolds number, and can be presented graphically as shown in Fig. 3.24, whence the factor

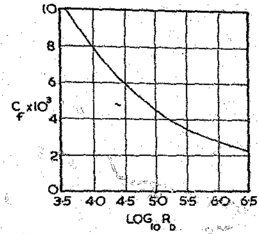


FIG. 3·24 SKIN FRICTION COEFF. FOR PIPE.

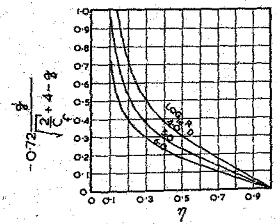


FIG. 3·25 CENTRE LINE DISPLACEMENT FACTOR FOR PIPE

$$\frac{0.72\, g'}{\sqrt{\frac{2}{c_f}} + h - g}$$

can be expressed in terms of $\eta = \frac{\bar{y}}{R}$ and $R_D$, $y$ being the distance from the duct wall. Thus, the above factor can be presented in terms of $\eta$ by means of a family of graphs for different values of $R_D$ (Fig. 3.25) yielding values for the correction factor $\frac{\bar{U}_d}{\bar{U}}$ for typical practical values of $\frac{d_p}{D}$ as defined by equation (3.20).

Applying this method to a spherical probe of diameter 0.3 inch, operating in a duct of, say, 8-inch diameter the value of $\frac{\bar{U}_d}{\bar{U}}$ on the duct centre line is unity, while the correction factor for a point 0.8 inch from the wall, at a Reynolds number of $10^6$, is approximately 1.006 or 0.6 per cent.[47] The latter correction seems too high.

This example is cited to illustrate a method of estimating a correction factor for the displacement error. For spherical probes, however, equation (3.20) would probably not be applicable because the 'Young and Maas' factor of 0.18 would probably not hold for the changed probe geometry.

The internal configuration of spherical probes -

where flow takes place through the probe and round a central cylinder, which houses the pressure orifice - is not exactly comparable to the conventional pitot-tube type of instrument which has a stagnation point at the instrument tip. Therefore displacement errors for probes with spherical shields must be studied and analysed separately following the method described above.

## 5. APPLICATION OF THE SPHERICAL PROBE

At the beginning of this chapter the necessity for the development of an improved-type total pressure probe was emphasized. The Kiel probe has so far been the only instrument capable of measuring total pressure accurately in strongly three-dimensional flow; it is, however, clear from its construction that it is difficult to produce several identical small instruments. The National Advisory Committee for Aeronautics has tested these instruments,[41] the size adopted being 1 inch overall diameter. For flow surveys inside turbo-machines and in the small passages sometimes encountered in fluid mechanics investigations, a probe of 1 inch diameter is too bulky. It is known that, in turbo-machinery, flow inclinations can be as high as 45 degrees.[36] It was impossible to conduct total pressure surveys in a strongly three-dimensional flow field with these conventional instruments, owing to very limited ranges of insensitivity to angular flow. The spherical probe which has been described seems to bridge this gap.

The author is of the opinion that the performance of this probe could be improved even further if in the manufacturing process the drilling out of the internal probe contours could be performed in one operation on a purpose-made drill-head. Abrupt changes in internal contours and burrs could be altogether avoided with the result, as the experimental trend indeed indicated, that angular insensitivity range could be increased to ± 50 degrees, or more.

## 6. MEDICAL APPLICATION

In Chapter II it was reported that the author is at present assisting two heart specialists, attached to the Heart Unit of the University of Pretoria, in an attempt to isolate static pressure from total pressure measurements in blood flow.

When a catheter is inserted into the heart or vein it does not register true total pressure because of the orientation of the catheter opening relative to the direction of blood flow. An instrument tip which is insensitive to angle of flow direction is required so that true total pressure would be registered. The author accordingly proposed that a small spherical probe be constructed (as small as practically possible) and fitted on to a catheter tip. The instrument characteristics are to be determined in blood flowing in a one-inch diameter transparent pipe in a circulatory system in the laboratory. The high viscosity of blood might impose a size limitation on the probe for reasonable reaction time. Should this be so, a small pressure transducer, built in behind the probe head in the lead, might have to be considered.

The Heart Unit recently acquired an instrument for accurate determination of flow volume by the 'gulp' method, described in Chapter II. It is proposed to determine the total pressure in the heart chambers or in a vein, after which the flow volume and hence the velocity can be estimated by the 'gulp' method. The static pressure can then be computed by subtracting dynamic pressure from measured total pressure. Thus :

$$p_s = (p_s + \tfrac{1}{2}\rho\bar{V}^2) - \tfrac{1}{2}\rho\bar{V}^2$$

$$\text{or } p_s = p_t - \tfrac{1}{2}\rho\bar{V}^2$$

In the calibration tests referred to earlier, it is proposed, as a check, to determine the static pressure as described above and to compare the results with those obtained from wall static tappings on the transparent pipe in the laboratory circulatory system.

Application of the spherical total pressure probe in the medical field seems promising and if the tests prove successful the improved catheter will be of tremendous assistance in cardiac and circulatory research and diagnosis.

## 7. CONCLUSION

Two types of miniature total pressure probe having spherical shields have been developed. The instruments showed highly satisfactory performance characteristics, comparable with those of the original Kiel and cylindrical probes. The instruments are much simpler to manufacture than the Kiel and cylindrical shielded probes and are more stable. The theoretically determined performance characteristics were confirmed experimentally and factors affecting the accaracy of measurements made with this instrument have been analysed.

The author trusts that the development of the spherical total pressure probe will constitute a significant forward step in the field of total pressure measurement in strongly three-dimensional flows or in flows involving large angles of attack.

## CHAPTER IV

## THE MEASUREMENT OF STATIC PRESSURE

### INTRODUCTION

In Chapter I present-day methods for measuring static pressure were briefly reviewed. As pointed out, static or piezometric pressure in a field of flow is that pressure which would act on, and be indicated by, a pressure registering device if it were moving along with the stream so as to be at rest or relatively 'static' with respect to the fluid. To design an instrument which will record this pressure accurately in accordance with the above definition has, as yet, not been possible.

Static pressure is a most useful parameter in fluid mechanics for it is directly related to density, temperature, fluid acceleration and velocity. Customary methods employed for measuring this pressure are the following :

(a) Wall static tappings or piezometer holes drilled through a duct wall perpendicular to the direction of flow;

(b) static pressure orifices located on a total pressure probe, viz. the pitot-static tube;

(c) single purpose instruments, viz. cylindrical probe with static pressure orifices. These instruments measure static pressure only.

Where high accuracies are required none of the methods referred to above is entirely satisfactory. In the following section the author attempts to show why.

## 2. PROBLEMS ASSOCIATED WITH STATIC PRESSURE MEASUREMENT

At present, there are still many complex factors affecting the measurement of static pressure, irrespective of the method employed.

When a small hole is drilled at right angles into the wall of a duct carrying a fluid, the pressure observed at such a piezometer tapping is a fair measure of the local static pressure, provided that the hole-geometry and internal hole finish meet certain requirement. Uncertainty and speculation among leading authorities concerning these requirements, together with the difficulties encountered in satisfying them in practice, result in errors in measurement.

Due to the hole-effect, the possibility of slight suction or impact pressures is always present even in the ideal piezometric tapping.

The problem of the static hole error has been investigated by : Fuhrmann (48) (1912), Hermann (49) (1929), Allen and Hooper (50) (1932), Myadzu (51) (1936), Rayle (52) (1949), Ray (53) (1956), Shaw (54) (1959), Stratford and Ascough (18) (1960) and Livesay, Jackson and Southern (55) (1962). These authors carried out experiments under widely varying conditions and experimental procedures as well as with different operating fluids and apparatus. Their findings could be summarised, as reported by Livesay et al, (55) by stating that the trends of different wall static hole effects have been established, although marked disagreement about their magnitudes and true interrelationships still exist.

Static pressure measurements by means of a conventional pitot-static tube are subject to errors caused by disorientation between pitot cylinder and flow direction; in addition, the positions of zero dynamic pressure on the cylindrical surface tend to shift away from the static orifices with increasing Reynolds number, probably due to probe boundary-layer effects.

Attempts have been made to develop single-purpose probes. A typical design is one in which the pressure is measured at an orifice drilled centrally in one face of a thin disc the plane of which is set parallel to the direction of flow. Misalignment and unknown hole-and Reynolds number effects are clearly sources of error. The needle probe and the two-hole pitot cylinder and pitot sphere, which are also employed as single-purpose instruments, have similar disadvantages. Also, turbulence and swirl cause errors in measurements. The effects and interdependence of these factors remain sources of speculation; further analytical work and instrument development are clearly necessary.

In this chapter the most commonly applied techniques are dealt with, and the present level of knowledge of the various factors affecting the three methods referred to are analysed separately with the object of clarifying static pressure measurement. Correction factors are suggested and finally the fundamentals of a spherical single-purpose static pressure probe, which was developed by the author, are described.

## 3. WALL STATIC TAPPINGS

The following factors affect static pressure measurement:

3.1 Static hole geometry.
3.2 The inherent static hole error.
3.3 Internal finish of tapping.
3.4 Rounded internal corners of tapping hole.
3.5 Method of pressure tapping.

3.6 Variation of static pressure over a cross-section due to turbulence.

Considering the above factors it is clear that the effects of hole geometry, internal finish and rounded internal corners combine to precipitate the inherent static hole error. However, due to the considerable volume of experimental work covering these individual factors, it was decided to analyse them separately.

3.1 <u>Static hole geometry</u>

The diameter of a static hole tapping has a marked influence on the determination of static pressure. If the diameter is too large, boundary fluid filaments split up and impinge on the fluid in the hole, causing a pressure above that of the true static.

Irregular roughness in the vicinity of a hole and sharp edges cause fluid filaments to separate from the walls, thereby indicating a pressure lower than the true one. If a tapping diameter is much greater than the pipe wall thickness, stream filaments entering the hole are split up and the result is an increase of pressure due to the formation of stagnation points. Depending on pipe roughness and diameter, there is an optimum diameter of tapping hole.

Preston and Norbury (7) found that at a Reynolds number of $4 \times 10^4$, for a discharge error of 0.1 per cent, the maximum allowable hole size was 0.055 inch in air flow and 0.095 inch in water flow. They also reported that, for a given Reynolds number, hole size was inversely proportional to the mean velocity.

According to information derived from Russian practice, maximum static hole size for air flow is 0.083 inch while that for water is limited to 0.4375 inch.

American practice (56) prescribes rather outsized static hole sizes, ranging from 3/8 inch to 3/4 inch, for pipes from 4-inch to 8-inch internal diameter, and 1/2 inch to 1 inch for pipes having internal diameters of 10 inches and more. The differences in standards, and therefore accuracies, are self-evident. The author is of the opinion that static hole diameters greater than 0.25 inch, even in large pipes, can lead to serious errors.

Stratford and Ascough (18) determined the best hole size experimentally by drilling out with great care and precision a dozen identical wall plug static holes of 0.063 inch diameter. In these holes, four plugs having hole sizes varying from 0.011 inch to 0.063

inch were tested. The tests provided data on the effect of static hole diameter which agreed well with Shaw's [57] suggestions for hole diameter correction and are dealt with later.

The same authors found by calculations that static pressure variation across a boundary-layer was negligible and confirmed by static probe traverse that static pressure throughout the main stream was constant. These results would, of course, be applicable only to specific flow conditions and will also be discussed later. They also claim that, provided the flow is steady, static pressure can be determined to within 0.1 per cent of the dynamic head by employing four 'high quality' holes, corrected for hole size. In practical engineering, however, meticulous attention to wall static orifices is not always possible and steady flow conditions are rarely encountered.

The American Society of Mechanical Engineers (A.S.M.E.) Code on fluid meters [56] concedes that, whatever the hole size, 'the possibility of a slight suction always exists'. This would cause a lower static pressure to be measured. According to the above evidence, this statement is in error and would be true only if separation at an orifice edge occurs.

In reference (56), it is stated that : 'If the stream is turbulent and full of eddies, the pressure in the side hole (static orifice) will fluctuate irregularly; but, under all ordinary circumstances, these fluctuations will be too small or too rapid to affect the gauge which will indicate the average pressure in the side hole'. Such an approach is unlikely to lead to improvement in the accuracy of static pressure measurement.

Another important requirement in static orifice geometry is that a tapping diameter should not change for a distance of at least 2.5 times the diameter of the hole as measured from the internal pipe face. It has been established experimentally that to ensure reliable results, this distance should, wherever possible, be made equal to from three to five times the diameter of the hole.[55]

Livesey et al [55] have shown experimentally that if a hole has a cavity behind it, reduction of hole depth is accompanied by a reduction in the error. They also reported negative errors for holes having depth/diameter ratios lower than about 2. In the Reynolds number range $0 \leq R_d \leq 300$ (based on orifice hole diameter), these authors found that a clean sharp-edged hole, with a depth/diameter ratio of about 2.5 and a cavity expansion ratio of approximately 14, will measure a pressure very close to the true wall static pressure.

The depth-effect of a hole seems to be reduced as the expansion ratio is decreased.

Further investigations on the effects of hole, depth, and cavity dimensions are therefore necessary. This, as well as the correction due to hole size, is dealt with in the next sub-section.

## 3.2 The inherent static hole error

In the previous sub-section it was shown how a static hole, which causes discontinuity in a pipe wall affects flow filaments in the boundary layer which, in turn, alter the true value of the local static pressure. A rigorous mathematical evaluation of the resulting error has not yet been possible, and accurate experimental determination of the magnitude of the possible error has been hampered by the lack of suitable methods for measuring the exact datum static pressure level.

On the assumption that the static hole error is caused by a disturbance in the flow field close to a solid boundary, the author, employing dimensional analysis, developed a functional relationship between pressure correction and Reynolds number (expressed in terms of friction velocity and hole diameter) which is given by :

$$\Delta_p = f\left(\frac{u_f \rho d_s}{\mu}\right) \quad \ldots\ldots\ldots\ldots\ldots\ldots\ldots \quad (4.1)$$

where,

$\Delta_p$ = difference between true wall static pressure and that actually measured;

$u_f$ = friction velocity $= \sqrt{\frac{\tau_w}{\rho}}$ ;

$\rho$ = mass density of fluid;

$d_s$ = diameter of static pressure orifice;

$\mu$ = fluid viscocity;

$\tau_w$ = wall shear stress.

At this point, the author started hunting for related experimental data in an attempt to evaluate equation (4.1). Subsequently papers by Preston and Norbury, (7) Shaw, (57) Livesey et al (55) and Oosthuizen (47) came to the author's notice. Both Shaw and Livesey developed expressions identical to equation (4.1) and although the exact experimental relationship has not yet been determined, both authors produced approximate curves based on available experimental data. A type of S - form curve, as determined by Livesey et al (55) is shown in Fig. 4.1. This curve differs from the Shaw function which has a more pronounced S shape as shown.

Considering the mean error as predicted by Shaw and Livesey et al, these results would probably give a static hole error to within 20 per cent of its true

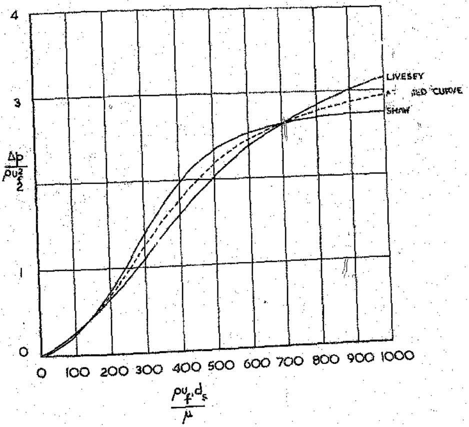


FIG. 4·1. ASSUMED STATIC HO..E ERROR

value [55] and the author submits that although, in the absence of a reliable static pressure datum, this statement cannot be verified experimentally, the application of this approximate function should reduce the static pressure error.

In order to use the abovementioned results, equation (4.1) is expressed as :

$$\frac{\Delta p}{\rho u_f^2} = F \left[\frac{u_f \rho d_s}{\mu}\right] \quad \text{..................(4.2)}$$

This relationship is shown in Fig. 4.1 as the assumed correction curve.

The part in brackets in equation (4.2) can be expressed as :[47]

$$\frac{u_f \rho d_s}{\mu} = R_D \sqrt{\frac{C_f}{2}} \cdot \frac{d_s}{D}\text{, and}$$

hence equation (4.2) becomes :

$$\frac{\Delta p}{\rho u_f^2} = F \left[R_D \sqrt{\frac{C_f}{2}} \cdot \frac{d_s}{D}\right] \quad \text{....(4.3)}$$

where,

$R_D$ = pipe Reynolds number based on pipe diameter;

$C_f$ = local coefficient of skin friction defined as

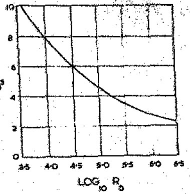


FIG. 4·2. SKIN FRICTION COEFF. FOR PIPE

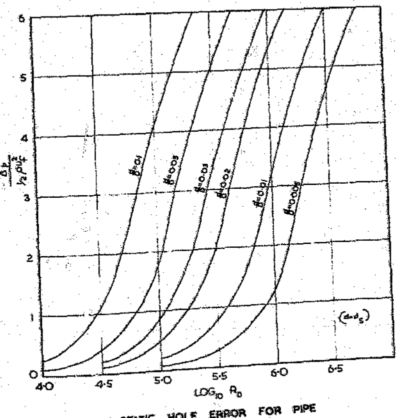


FIG. 4·3. STATIC HOLE ERROR FOR PIPE

$$C_f = \frac{T_w}{\frac{1}{2}\rho U_m^2} \quad \text{and}$$

$U_m$ = mean conduit velocity.

Now $C_f$ can be expressed in terms of $R_D$ and the curve representing this experimental relationship is shown in Fig. 4.2. By means of the curves in Figs. 4.1 and 4.2, equation (4.3) can be evaluated to give the average correction factor for practical values of $\frac{d_s}{D}$ at various Reynolds numbers. Thus a family of correction curves can be drawn as shown in Fig. 4.3.

From these results it follows that a reasonable correction can be applied to any wall static pressure reading, in a particular pipe, depending on the hole size and the Reynolds number, or that the maximum value of a static orifice diameter can be determined in order to attain a specified limit of accuracy.

It is necessary to point out, however, that the successful application of this correction method depends on considerable additional experimental work. There is, at present, some doubt about the exact shape of the S curve, especially near the origin. Theoretically the gradient of the curve near the origin should be zero, thus substantiating the presently accepted S form. Shaw's[57] experiments confirmed the shape of the curve near the origin. Stratford and Ascough [18] reported such a wide

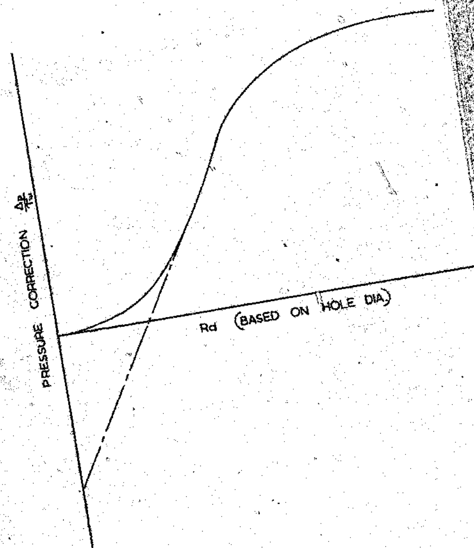


FIG.4.4 STATIC PRESSURE ERROR DUE TO HOLE SIZE

scatter near the origin that it was impossible to determine the exact shape of the curve. Rae [53] obtained a curve showing an almost linear relationship near the origin (Fig. 4.4), and Lester [55] confirmed this shape. The most recent work by Livesey et al [55] produced yet another curve, as shown in Fig. 4.1, having a very flat S shape which, in fact, approximates a flat parabola near the origin. This part of the curve was however obtained by extrapolating to zero hole size in accordance with the assumption that the static hole error might be proportional to the mean dynamic pressure in the undisturbed flow in the boundary-layer. This hypothesis, which still awaits rigorous corroboration, does not seem unreasonable.

Applying this approximate S curve, Oosthuizen [47] calculated corrections for static pressure readings in boundary-layer flow at high Reynolds numbers, in fully developed flow in a pipe, and in a two-dimensional channel, differentiating between the 'inner' or 'universal' and 'outer'* flow regions. The difference between a static hole correction for 'inner' and 'outer' regions in pipe flow is, however, not appreciated. The correction due

* The 'inner' or 'universal' region is the flow zone near a pipe wall in which viscous shear stresses are as important as turbulent stresses or predominate. The 'outer' region occupies all but the region very close to a wall and here turbulent shear stresses predominate.

to turbulence, which is dealt with in the following paragraph, would be different for the two regions but the static hole correction is surely not affected by the difference between the velocity distributions for the 'inner' and 'outer' regions.

For determining the shape of the S-function near the origin in order to define its present approximate form more precisely, the author suggests the following experimental procedure :

Attempts to correlate experimental results on the lines dictated by dimensional analysis is a fairly recent development and should form the basis of future experimental work. The main difficulty in previous investigations seemed to be that of estimating true static pressure at the wall from measurements of wall static pressure at tapping points of various diameters, and by extrapolation to zero hole size. Calculation of the true wall static pressure from a series of accurately determined experimental parameters instead of extrapolating in a region where the results are subject to maximum errors due to the small tapping hole sizes, seems to be the preferable alternative.

The total pressure in a boundary-layer can be determined fairly accurately by means of special boundary-layer total pressure probes. The newly-developed 'hot-film' technique (58) could then be employed and velocity patterns, close to a pipe wall in the boundary-layer, could be measured to greater accuracies than those given by the existing 'hot-wire' methods. From these measured velocities the total pressure, as measured, could (if necessary) be corrected for turbulence and the dynamic pressure head determined, from which the true static pressure close to the pipe wall could be calculated to reasonable accuracy. This method would probably yield a more reliable error function, or B-curve, when the results are correlated with measured wall static tapping values. The error correction due to this factor will be dealt with again when considering venturi meters in Chapter VI.

3.3 Internal finish of tapping hole

Tapping hole finish, after drilling, must be controlled with great care. Roughness effects in a pipe wall are also important in the immediate vicinity of a hole, and it is essential that static orifices should be free from burrs. Shaw[57] drew attention to the fact that errors caused by small burrs may be several times greater than those due to finite tapping hole size. For accurate measurements, reaming on the internal edges is imperative and when a relatively small hole size is used in big pipes, with high roubgness coefficients, the internal pipe wall should be smoothed immediately upstream and downstream of a hole. Burrs tend to shed myriads of small eddies which, when superimposed on the main flow near a hole, cause secondary turbulence effects and increased error.

The author submits that 'tapping hole manufacturing' could be improved considerably and possibly standardized if plugs were made separately. This would ensure the necessary meticulous attention to finish; these plugs could be fitted into a pipe through a boss such that no edges or burrs existed between the internally prepared pipe surface and the internal plug profile.

3.4 <u>Rounded internal tapping hole corners</u>

If the internal hole corners are rounded excessively, secondary flow occurs in the immediate hole entrance causing impact which tends to increase true local static pressure.

Most investigators prescribe a 'small' or 'reasonable' rounding of the internal edge without attempting to specify the radii. Work at Liverpool University (17) seems to indicate that a 'slight' rounding to a radius of one-tenth of the tapping hole diameter is desirable. Neale (17) used a radius of

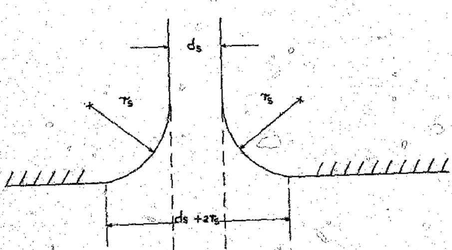


FIG. 4·5 WALL STATIC TAPPING WITH ROUNDED ENTRANCE.

one-quarter the hole diameter but gave no reason for choosing this particular ratio. The A.S.M.E. Code prescribes radii which apparently have no fixed relationship to hole diameter. Neale's values, as well as those specified by the A.S.M.E. Code, seem high when compared with the findings at Liverpool University.

Livesey et al.[55] on the other hand reported that a hole with radiused edge gave a larger error than one with a sharp edge free from burrs, whereas a hole with chamferred edge showed a reduced error. Clearly, the effect of this factor remains a source of speculation.

Further theoretical and experimental work would therefore be of considerable assistance. It would probably be advisable to select a deep hole of diameter, $d_s$, and to adjust this at entrance to a slightly higher value to allow for the effect of a particular rounding radius, $r_s$. The static hole diameter to be used would then be $d_s' = d_s + 2\ r_s$, instead of $d_s$. See Fig. 4.5. The author's assumed correction curve (Fig. 4.1) could then be applied to these adjusted orifice diameter values in an attempt to establish the best relationship between $d_s$ and $r_s$. It should be observed, however, that the rounding radius is, in effect, analogous to an increase in static orifice diameter, and therefore these results should be compared with those obtained from identical sharp-edged orifices. If a more reliable static pressure datum could be calculated, as proposed, the doubt concerning the error effect of this factor could probably be eliminated.

## 3.5 Method of pressure tapping

Pressure can be sensed by means of :

3.5.1 A single tapping point in a pipe wall;

3.5.2 a number of orifices distributed symmetrically around a pipe circumference; or

3.5.3 piezometric slots or rings over the whole or part of a pipe perimeter.

When flow is sufficiently 'straight' at any section, i.e. at low turbulence level, so that the static pressure remains sensibly uniform over the stream cross-section, the average static pressure can be measured by means of a single wall static orifice. However, these ideal conditions very seldom obtain in practice.

Should the turbulence level be such that a circumferential static pressure variation exists, method 3.5.2 above must be employed to determine the best average value of the static pressure over a cross-section. This method is the better alternative in ordinary field and laboratory applications.

With a view to improving average static pressure measurements in turbulent flows, method 3.5.3 above is often employed. If, however, the pressure at points around a circumference differs appreciably, circulation through a circumferential ring will result, and an erroneous static pressure will be registered at the 'lead-off' point in the ring.

In the discussion on reference (8), Winternitz referred to a thesis on static pressure measurement, submitted to the University of Göttingen by Krause, dealing with pressure measurement by means of slotted orifices. The results revealed that corrections were almost negligible in the absence of a pressure gradient in the direction of flow. At a position 0.11L from the leading edge of a slot of length L, the correct static pressure was measured provided the Reynolds number, based on slot width, was less than 60. Stratford (8) pointed out in the discussion that accurate manufacture of the slot-type tapping would prove difficult in practice. It is also clear that in the higher range of Reynolds numbers the slot width for a slot Reynolds number of less than 60 would be prohibitively small.

However, the slot tapping method does not appear to be without merit and further theoretical and experimental analysis seems justified.

3.6 Static hole error due to turbulence

When the stream tubes of flow in a pipe are straight and parallel, static pressure is uniform over a normal cross-section. If stream tubes are curved, however, static pressure increases from the inside to the outside of a curve due to the effect of centrifugal force.

Turbulence and eddies in a stream can be considered as a complex structure of curved currents superimposed on the general flow pattern or motion, causing local variations of static pressure over a pipe cross-section.

In turbulent flow the true static pressure at a wall static tapping would differ from that at a point distant y from a pipe wall. Another factor often overlooked is the difference between the true average wall static pressure and the true average static pressure over a pipe cross-section. This difference is of particular importance in the measurement of throat and upstream static pressure in a venturi meter.

The Navier-Stokes equations, expressed in cylindrical co-ordinates, can be applied to this problem for fully developed pipe flow; the second momentum equation yields : (59)

$$\frac{p_w - p_s}{\rho\, u_f^2} = \frac{\Delta' p}{\rho u_f^2} = \int_0^{\bar{y}} \frac{\frac{\overline{v'^2}}{u_f^2} - \frac{\overline{v'^2}}{u_f^2}}{1 - \bar{y}}\, d\bar{y} + \frac{\overline{v'^2}}{u_f^2} \quad \ldots\ldots\ldots\ldots (4.4)$$

where $p_s$ = true static pressure at a point distant $y$ from the pipe wall;

$p_w$ = true static pressure at wall tapping;

$u_f$ = friction velocity, $= \sqrt{\frac{\tau_w}{\rho}}$,

$\bar{y}$ = $\frac{y}{r}$, where $r$ = pipe radius, and

$v'$ and $w'$ = turbulent velocity fluctuations.

This correction equation can be evaluated from Laufer's experimental results, which give the turbulence structure in a pipe (42) and in a two-dimensional channel. (60)

In velocity traverses in pipe flow for example, a total pressure probe and wall static tappings can be employed more accurately if the static pressure, as measured, is corrected for hole size as well as for turbulence, the latter correction depending on the position of the total pressure probe relative to the pipe wall.

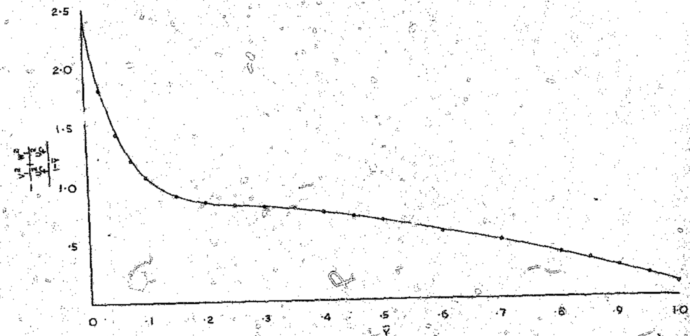


FIG. 4.6 TURBULENT VELOCITY COMPONENTS IN A PIPE (FROM LAUFER'S RESULTS).

This static pressure correction can thus be expressed as :

$$\frac{\Delta p + \Delta' p}{\rho u_f^2} = F\left[R_D\sqrt{\frac{C_f}{2}} \cdot \frac{d_s}{D}\right] + \int_0^{\bar{y}} \frac{\frac{\overline{w'^2}}{u_f^2} - \frac{\overline{v'^2}}{u_f^2}}{1 - \bar{y}} \cdot d\bar{y} + \frac{\overline{v'^2}}{u_f^2} \quad \text{.............. (4.5)}$$

In equation (4.5), $\Delta_p$ can be determined from F ,3 as shown earlier, while $\Delta'_p$, the turbulence error component, can be evaluated from Laufer's data as shown in Figs. 4.6 and 4.7.

As stated earlier, the term for turbulence correction in the above equation should, strictly speaking, be evaluated as a turbulence factor for the 'inner region' added to that for the 'outer region', due to the difference between the turbulence structure in these regions. In most practical cases of pipe flow, however, the effect of discrepancies in root mean squared values of velocity fluctuations in these regions is so small that this refinement may be neglected at the present stage of development. As more accurate experimental data on turbulence structures for different flow fields become available, the application of correction equation (4.5) should yield more accurate results.

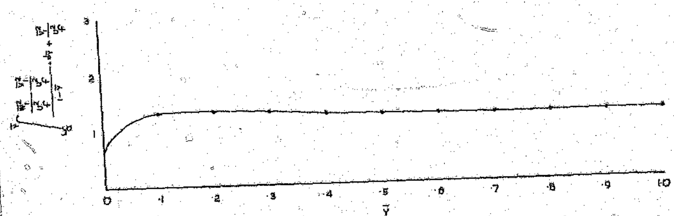


FIG. 4.7 TURBULENCE CORRECTION FOR WALL STATIC TAPPING

A correction which has apparently been overlooked until now is that for the average static pressure over a cross-section of a pipe, say, relative to the wall static pressure measurement in turbulent flows. At the entrance and throat sections of a venturi meter, for example, the static pressures as measured by a series of wall static tappings are considered as the average values for these sections, irrespective of the variation of static pressure over a pipe cross-section.

Neglect of this correction would, of course, affect experimentally determined values of the discharge coefficient $C_d$.

The assumed ideal static pressure distribution over a cross-section of turbulent flow in a pipe is shown in Fig. 4.8. It follows that the mean static pressure over the cross-section is given by :

$$\overline{p_s} = p_w - \overline{\Delta'_p} \qquad \text{.................. (4.6)}$$

where $\overline{\Delta'_p}$ represents the average value of the turbulence correction over the pipe cross-section. At any point distant $\overline{y}$ from the pipe wall, the static pressure, $p_s$, will be less than the wall static pressure, $p_w$, by an amount $\Delta'_p$, where $\Delta'_p$ is defined by equation (4.4). The value of $\Delta'_p$ can be determined thus :

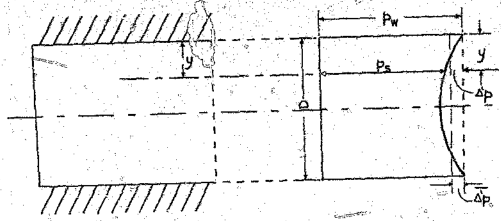


FIG. 4·8 IDEAL STATIC PRESSURE DISTRIBUTION OVER PIPE CROSS SECTION FOR TURBULENT FLOW.

$$2 \pi \int_0^r \Delta'_p \, (r - y) \, dy \; = \; \Delta'_p \, . \, \frac{\pi D^2}{4} \quad \ldots\ldots\ldots\ldots (4.7)$$

writing, as before, $\overline{y} \; = \; \frac{y}{r}$, we have :

$$dy \; = \; r \, . \, d\overline{y}$$

and hence equation (4.7) becomes :

$$2\pi r^2 \int_0^{\overline{y}} \Delta'_p \, (1 - \overline{y}) \, . \, d\overline{y} \; = \; \Delta'_p \; . \; \frac{\pi D^2}{4}$$

$$\text{or} \quad \overline{\Delta'_p} \; = \; \frac{8r^2}{D^2} \int_0^{\overline{y}} \Delta'_p \, (1 - \overline{y}) \, . \, d\overline{y} \quad \ldots\ldots\ldots\ldots (4.8)$$

Substituting equation (4.4) in equation (4.8) yields :

$$\frac{\overline{\Delta'_p}}{\rho u_f^2} \; = \; 2 \int_0^{\overline{y}} (1 - \overline{y}) \left[ \int_0^{\overline{y}} \frac{\dfrac{\overline{v'^2}}{u_f^2} - \dfrac{\overline{w'^2}}{u_f^2}}{1 - \overline{y}} \, . \, d\overline{y} + \frac{\overline{v'^2}}{u_f^2} \right] . \, d\overline{y} \quad \ldots (4.9)$$

From Laufer's [42] experimental determinations of the root mean squared values $\sqrt{\overline{v'^2}}$ and $\sqrt{\overline{w'^2}}$ for fully developed pipe flow, the term in square brackets in equation (4.9), i.e. $\Delta'_p$, have been evaluated for different values of $\overline{y}$ as shown in Fig. 4.7 and hence $\Delta'_p \, (1 - \overline{y})$ can be determined for different values of $\overline{y}$, from which equation (4.9) can be evaluated by graphical integration. The result is shown in Fig. 4.9 from which it follows that :

$$\overline{\Delta'_p} \; = \; 1.26 \, . \, T_\omega \; = \; C \, T_\omega \quad \ldots\ldots\ldots\ldots (4.10)$$

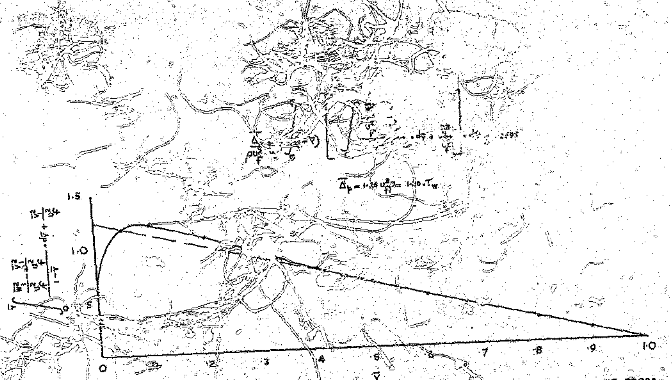


FIG. 4.9 TURBULENCE CORRECTION FACTOR FOR AVERAGE STATIC PRESSURE OVER A PIPE CROSS-SECTION.

Thus $\overline{A}_p^*$ can be determined for a particular friction velocity $U_f$ and from equation (4.6) the true average static pressure over a pipe cross-section under conditions of turbulent flow can be estimated.

The foregoing discussion reveals how the differential pressure measurement in a venturi meter is affected. If, as a first approximation, the turbulence structures in the throat and at entrance to a venturi meter are assumed to be approximately of the same form, the constant, C, in equation (4.10) would be identical for the entrance and throat sections:

Thus

$$\overline{A}_p^* \text{ (throat)} = CT_w^*, \text{ and}$$

$$\overline{A}_p^* \text{ (entrance)} = C\,T_w$$

The need for corrections would therefore not be eliminated when a pressure difference is considered because the values of $T_w$ and $T_w^*$ at the two sections are different. The effect of this correction in a theoretical expression for the discharge coefficient of a venturi meter will be dealt with in Chapter VI.

As stated earlier, evaluation of the foregoing corrections is possible only if reliable experimental data on the root mean squared values of the velocity fluctuations in various appropriate turbulent flow regimes are available.

4. STATIC PRESSURE ORIFICES IN THE PITOT-STATIC TUBE

Static pressure can also be measured by correctly placed orifices in spheres or cylindrical tubes. If a sphere or a cylinder is correctly oriented in a flow field - the cylinder axis being either parallel or perpendicular to the direction of flow - total pressure will be registered at the stagnation point. A study of the pressure distribution around such bodies reveals that somewhere between the stagnation point and the negative or suction pressure zone a 'neutral position' exists where a small orifice would register, approximately, the static pressure in the fluid; this position is approximately 40 degrees from the stagnation point.

Theoretically, an open-end tube held with its axis perpendicular to the direction of fluid motion should register the true static pressure. In practice, however, the fluid does not move tangentially past the opening, but actually forms convex flow lines at and within the opening, thereby causing centrifugal suction. On the other hand, a pressure increase can result from within the opening. The mere provision of an orifice at the correct position, with its axis normal to the direction of flow at the particular point, therefore, does not solve the problem.

The factors affecting static pressure measurement by suitable orifices on spherical or cylindrical probes, can be listed as :

4.1 The error due to inappropriate size of orifice;

4.2 the shift of the neutral position on the probe body with increased Reynolds number;

4.3 misalignment of probe with direction of flow;

4.4 the boundary-layer formed on the probe itself;

4.5 the effect of turbulence..

4.1 Inappropriate orifice size

Just as the presence of a small piezometer hole in a pipe wall causes an error in a wall static pressure measurement, so also a comparable effect is likely to be associated with an orifice on a probe face. Assuming that the static hole error is caused by a disturbance in the flow in the boundary-layer on the probe, an expression identical to equation (4.2) can be developed, i.e.

$$\frac{\Delta_p^p}{\rho u_f^2} = F \left[ \frac{u_f \rho d_s^p}{\mu} \right] \quad \ldots\ldots\ldots\ldots\ldots\ldots (4.11)$$

where $\Delta_p^p$ = static pressure error due to the static hole size on a probe, and

$d_s^p$ = diameter of static hole, the other symbols having their usual meanings.

To evaluate equation 4.11 requires experimental investigations. The total pressure in the probe boundary-layer must first be determined by means of a miniature total pressure probe. By 'hot-film' technique, velocity profiles close to the probe face could be surveyed and from these the static pressure could be calculated. By correlating the calculated with the measured probe values, an error curve could probably be constructed to give the probe static hole error for a particular instrument. Nowhere in literature on this subject could the author find any evidence of attention to this factor.

## 4.2 The shift of the neutral position

The position of the 'neutral point' on a spherical or a cylindrical face in a flow field tends to shift away from the stagnation point as the Reynolds number increases. This causes over-registration of static pressure because the positive pressure zone moves over

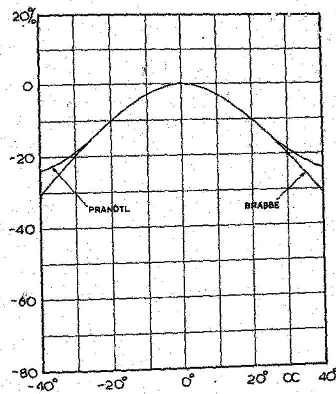


FIG. 4·10 ERROR CURVES FOR BRABBE AND PRANDTL TUBES the positions of the static orifices. In the higher Reynolds number ranges, the 'neutral point' also tends to oscillate about the position of the static orifices.

The degree of shift or oscillation is most probably controlled by the turbulence level, and could be caused by the complex interchange of energy between the laminar sub-layer and the turbulent boundary-layer on the probe. A form of boundary-layer control could perhaps minimize this effect, but such an approach would probably pose more difficulties than it solved. This factor will apparently always present an obstacle to static pressure measurement.

## 4.3 Probe alignment

One of the main sources of error results from the difficulty associated with aligning a probe accurately with the direction of flow. This is pronounced with the Prandtl and Brabbé tubes where the static orifices or piezometric slots are positioned on a cylindrical tube having its axis parallel to the flow direction.

If the instrument is inserted into a flow field, at an angle of yaw or pitch, the static pressure orifices register static pressure plus a component of the dynamic pressure. Fig. 4.10 shows the static error curves for the Prandtl and Brabbé tubes. These instruments have approximately identical sensitivity characteristics for angles of flow direction, the error being about -5 per cent at an angle of attack of ± 15 degrees. The limitations of these instruments when high accuracies are required, in two- and three-dimensional flow fields, are therefore self-evident.

4.4 The probe boundary-layer

The formation of a boundary-layer on a probe would affect the registration of static pressure. If, as was assumed, the static hole error is caused by a disturbance of the flow in the boundary-layer and if the probe boundary-layer controls the shift of the 'neutral point', this effect should be studied in detail by means of total pressure and velocity traverses. The effect on static pressure measurement of boundary-layer growth, stability and flow has not received the necessary attention and although the experimental obstacles associated with such an investigation would be considerable, a fundamental study of this nature seems to be essential.

4.5 The effect of turbulence

If a pitot-static tube is aligned with the main direction of flow in a turbulent flow regime, the u' fluctuating velocity component would not affect the static pressure whereas the v' and w' components would tend to increase the static pressure, depending on the actual flow directions of these turbulent components at the position of the static orifices. Expressed mathematically,

$$\Delta_p^t \quad = \quad K_t \rho \left[ \overline{v'^2} + \overline{w'^2} \right] \quad \ldots\ldots\ldots \quad (4.12)$$

where $\Delta_p^t$ = static pressure error due to turbulence, and

$K_t$ = constant to be determined depending on the directions of the turbulent fluctuating velocities.

A rigorous mathematical formulation of this effect is not yet possible, but Fage [59] suggested that a probe would overregister static pressure by an amount $\frac{1}{4}\rho \left[ \overline{v'^2} + \overline{w'^2} \right]$ in a turbulent flow field.

Thus equation (4.12) can be written as :

$$\frac{\Delta_p^t}{u_f^2} \quad = \quad \frac{1}{4}\rho \left[ \frac{\overline{v'^2}}{u_f^2} + \frac{\overline{w'^2}}{u_f^2} \right] \quad \ldots\ldots\ldots\ldots \quad (4.13)$$

In 1936, Fage suggested the above value of $K_t$ = 0.25 and, to the author's knowledge, no further attention was given to this factor.

Equation (4.13) can be written as :

$$\frac{1}{u_f^2 \rho K_t} \cdot \Delta_p^t = \left[ \frac{\overline{v'^2}}{u_f^2} + \frac{\overline{w'^2}}{u_f^2} \right] \quad \text{.........} \quad (4.14)$$

replacing Fage's constant of 0.25 by $K_t$.

Instead of separating the static pressure error due to orifice size and turbulence - the former would be very difficult to evaluate as pointed out earlier - one could perhaps consider the inherent orifice size error as being related to turbulence structure, and rewrite equation (4.14) in the form :

$$\frac{1}{u_f^2 \rho K} \cdot \Delta_p = \left[ \frac{\overline{v'^2}}{u_f^2} + \frac{\overline{w'^2}}{u_f^2} \right] \quad \text{...........} \quad (4.15)$$

where K is a correction constant and $\Delta_p$ is the total static pressure error i.e. due to turbulence and orifice size.

From Laufer's (42) data a curve can be constructed expressing $\frac{1}{u_f^2 \rho K} \cdot \Delta_p$ in terms of $\overline{y}$, where $\overline{y} = \frac{y}{r}$ as before.
It is evident that if $\Delta_p$ is determined experimentally, K can be evaluated from equation (4.15) for different positions $\overline{y}$. Thus, the 'best' value for static pressure at say a point on a pipe centre line can be determined by using a wall static tapping and correcting the